

RegQCNET: Deep Quality Control for Image-to-template Brain MRI Registration

Baudouin DENIS de SENNEVILLE¹, José V. MANJÓN²,
Pierrick COUPÉ³

¹ CNRS, University of Bordeaux, “Institut de Mathématiques de Bordeaux” (IMB), UMR5251, F-33400 Talence, France

² ITACA, Universidad Politecnica de Valencia Camino de Vera, s/n, 46022, Valencia, Spain

³ CNRS, University of Bordeaux, Bordeaux INP, “Laboratoire Bordelais de la Recherche Informatique” (LaBRI), UMR5800, F-33400 Talence, France

E-mail: bdenisde@math.u-bordeaux.fr, jmanjon@fis.upv.es,
pierrick.coupe@u-bordeaux.fr

April 2020

Abstract. Registration of one or several brain image(s) onto a common reference space defined by a template is a necessary prerequisite for many image processing tasks, such as brain structure segmentation or functional MRI study. Manual assessment of registration quality is a tedious and time-consuming task, especially when a large amount of data is involved. An automated and reliable quality control (QC) is thus mandatory. Moreover, the computation time of the QC must be also compatible with the processing of massive datasets. Therefore, deep neural network approaches appear as a method of choice to automatically assess registration quality.

In the current study, a compact 3D CNN, referred to as RegQCNET, is introduced to quantitatively predict the amplitude of a registration mismatch between the registered image and the reference template. This quantitative estimation of registration error is expressed using metric unit system. Therefore, a meaningful task-specific threshold can be manually or automatically defined in order to distinguish usable and non-usable images.

The robustness of the proposed RegQCNET is first analyzed on lifespan brain images undergoing various simulated spatial transformations and intensity variations between training and testing. Secondly, the potential of RegQCNET to classify images as usable or non-usable is evaluated using both manual and automatic thresholds. The latter were estimated using several computer-assisted classification models (logistic regression, support vector machine, naïve bayes and random forest) through cross-validation. To this end we used expert’s visual quality control estimated on a lifespan cohort of 3953 brains. Finally, the RegQCNET accuracy is compared to usual image features such as image correlation coefficient and mutual information.

Results show that the proposed deep learning QC is robust, fast and accurate to estimate registration error in processing pipeline.

Keywords: Quality Control, Image-to-template registration, Deep Neural Network.

1. Introduction

A wide variety of processing pipelines have been proposed in the literature to make automatic brain image analysis possible. Standardization of image location and intensity is usually a necessary prerequisite for functional (Cook et al. 2006) (Song et al. 2011) or structural studies (Wei et al. 2002) (Chaogan & Yufeng 2010). This is commonly achieved using suitable algorithms designed for: image-to-template registration (Tustison et al. 2014) (Jenkinson et al. 2012) (Collins et al. 1994), inhomogeneity correction (Tustison et al. 2010) (Sled et al. 1998), tissue-based or intensity normalization (Nyúl et al. 2000) (Friston et al. 1995). A visual human inspection of the data after each step of the processing pipeline is commonly employed to detect possible problems in the outputs. This visual quality control (QC) is unfortunately not feasible when a huge amount of imaging data is involved (typically more than several thousands scans). Consequently, with the rise of large-scale datasets, recent efforts are dedicated to the development of reliable QC metrics to detect artefacts specific to the imaging acquisition and analysis process (Alfaro-Almagro et al. 2018) (Kim et al. 2019).

Fig. 1 summarizes the context of the current paper: our study is focused on the image registration step, the later being a necessary prerequisite to co-register one or several brain scans onto a common space defined by a template image. In practice, mis-registered data are inherently encountered and a QC on the registration is needed (red box in Fig. 1) (Avants et al. 2011). A manual assessment is generally employed as a QC which is however a time consuming task. Random forest (Hessam et al. 2019) and convolutional neural network (CNN) (Eppenhof & Pluim 2018) have been proposed to quantify the registration accuracy for both parametric (*i.e.*, rigid, affine) and deformable registration in chest CT scans. The direct translation of these methods to large lifespan brain MRI with various diseases has still to be studied. Several methods have been proposed for MRI brain registration to template space. In (Fonov et al. 2018) a cross-entropy loss function is used as an objective function to train the deep neural network on a series of 2D control images. This method produces qualitative estimation (*i.e.*, good or not good) of the registration accuracy. In (Bannister et al. 2019) and (Dubost et al. 2019), a DICE metric between transformed and original organ contours is proposed as a surrogate of the registration quality. The use of an indirect metric (*i.e.*, DICE) estimated on an auxiliary task (*i.e.*, segmentation) does not provide direct quantitative information on registration accuracy. Moreover, this information can be corrupted by the segmentation error which is a complex task by itself. Finally, these last three methods produce metrics (binary decision or auxiliary DICE) that cannot express registration error in metric unit system. Consequently, no meaningful task-specific threshold on the mis-alignment amplitude can be defined by a user.

Our contribution is four-fold:

- (i) A compact 3D CNN is introduced to quantitatively estimate the mis-alignment between an image and a template. The proposed QC, referred to as RegQCNET

in this study, is quantitative and can be expressed using metric system units. Moreover, an efficient and robust training procedure robust is proposed. The inputs of the designed CNN are: the registered image and the reference template. Besides, it is demonstrated that RegQCNET meets computational requirements related to the inclusion of this QC step in any analysis pipeline.

- (ii) The robustness of the proposed RegQCNET is analyzed on lifespan brain images undergoing various simulated spatial transformations and intensity variations between training and testing.
- (iii) The potential of RegQCNET to classify images as usable or non-usable was evaluated using both manual and automatic thresholds. The latter were evaluated using several computer-assisted classification models (logistic regression, support vector machine, naïve bayes and random forest) using a cross-validation procedure. To this end we used expert’s visual quality control estimated on a lifespan cohort of 3953 brains as a gold standard.
- (iv) The RegQCNET accuracy is compared to usual image features such as image correlation coefficient and mutual information.

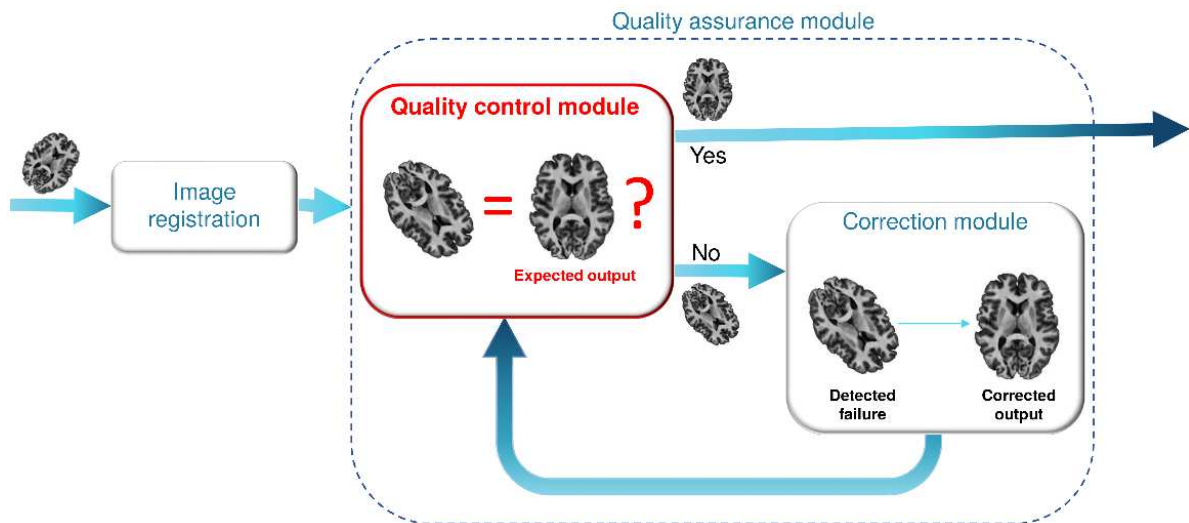


Figure 1: General principle of quality assurance on image registration. The current study aims at providing a Quality Control (QC) module (red box) designed to detect mis-aligned images. Note that the later can potentially be fed into an additionnal correction module (outside the scope of the current study).

2. Materials and Methods

2.1. Datasets

Throughout this study, we used 3 datasets — 1 for training/2 for testing — referred to as “Simulated training dataset”, “Simulated testing dataset” (these last two were built

using a lifespan dataset, for which synthetic affine transformations were applied) and “Real testing dataset”.

2.1.1. Preprocessing of input images. To standardize input orientations and intensities, all scans involved in this study were first preprocessed beforehand using the volBrain pipeline (Manjón & Coupé 2016) with the following steps: i) denoising (Manjón et al. 2010), ii) inhomogeneity correction (Tustison et al. 2010), iii) affine registration into the template space ($181 \times 217 \times 181$ voxels at $1 \times 1 \times 1$ mm³, the ICBM 152 Atlas template was taken as reference for registration (Fonov et al. 2011)), iv) manual human assessment of the registration as described in (Coupé et al. 2017) (Coupé et al. 2019), and v) tissue-based intensity normalization (Manjón et al. 2008). Finally, image intensities were normalized using z-scoring using the mean and standard deviation from the complete image field-of-view.

2.1.2. Simulated training&testing datasets. 360 T1-weighted MRI of cognitively normal subjects, subjects with Alzheimer’s Disease and subjects with Mild Cognitive Impairment were randomly selected under constraints from the dataset used in our previous BigData studies to build the lifespan dataset (Coupé et al. 2017) (Coupé et al. 2019). This dataset was based on 9 datasets publicly available (C-MIND, NDAR, ABIDE, ICBM, IXI, OASIS, AIBL, ADNI1 and ADNI2). From 1 to 90 years we selected 2 females (F) and 2 males (M) for each age (*i.e.*, 2F and 2M of 1 year old, 2F and 2M of 2 years old and so on). Therefore, we obtained a balanced group with 50% of each gender uniformly distributed from 1 to 90 years. This balanced selection is done to limit bias introduction in training and testing datasets and to make our QC method robust to age and gender of the input image.

All the 360 MRIs underwent a human quality control. For this set of images, all the image were considered as correctly aligned with negligible residual registration mismatch. The RMSE was thus considered to be equal to 0. We are aware that these images are not perfectly aligned and that negligible errors might be in these manually QC images. Considering these remaining errors equal to epsilon or zero do impact the rest of the study.

At this point, we have a set of 360 scans with standardized location and intensity. This set was split into two separate datasets (stratified/no redundant data): 300 scans were designed to build the “Simulated training dataset” and 60 scans were designed to build the “Simulated testing dataset”. This split was done under constraint to ensure well-balance of age and gender between both.

The “Simulated training dataset”. One can expect that the training set has to be populated densely enough in terms of both anatomical inter-subject variability and simulated spatial deformations. RegQCNET was trained using N scans (randomly selected with replacement from the 300 above-mentioned scans) undergoing simulated spatial transformations producing an uniform RMSE distribution in the interval

$[0, \text{MAX_RMSE}=100]$ voxels. We tested N -values in the following set: $\{100, 1000, 10000\}$. Note that the obtained training set may include several transformations for each patient for $N > 300$.

The “Simulated testing dataset”. This set was composed by 500 scans (randomly selected with replacement from the 60 subjects selected to build the testing data). That way, the obtained training and testing datasets include several transformations (≈ 8 in average) for each patient.

Simulated spatial affine transformations. To train and test the proposed QC, 3D spatial transformations — composed by translation, rotation and scale variations — were simulated. Ranges for X-, Y-, Z-translations, rotations around X-, Y-, Z-axis, X-, Y-, Z-scaling factors are detailed in the experimental section below. The RMSE was calculated for each simulated transformation. Let MAX_RMSE be an upper limit on simulated RMSE values. A set of spatial transformations with a uniform RMSE distribution in the interval $[0, \text{MAX_RMSE}]$ voxels was built. To this end, 3D spatial transformations composed by translation, rotation and scale variation, were simulated as follows:

- X-, Y-, Z-translations were randomly selected separately in the interval $[-100, 100]$ voxels,
- Rotations around X-, Y-, Z-axis were randomly selected in the interval $[-45, 45]$ degrees,
- X-, Y-, Z-scaling factors were randomly selected in the interval $[0.5, 1.5]$ (a factor of 1 being equivalent to no scaling),

These transformations are then applied using bi-spline interpolation to subjects randomly selected in the training and the testing datasets (see Fig. 3).

2.1.3. The “Real testing dataset”. The performance of the proposed RegQCNET was evaluated on a massive brain-MRIs data base ($N = 3953$) including cognitively normal subjects, subjects with Alzheimer’s Disease and subjects with Mild Cognitive Impairment. These 3953 MRIs are the remaining subjects from the large-scale cohort used in (Coupé et al. 2019) after removal the 360 cognitively normal subjects used to build the simulated training and testing dataset. Consequently, the real testing dataset contains pathological alterations unseen in the training dataset which is only composed of cognitively normal subjects. All the images were processed as in the proposed study and underwent to human quality control. A visual assessment was done by checking screen shots of one sagittal, one coronal and one axial slice in middle of the 3D volume using the volBrain reports (Manjón & Coupé 2016).

2.2. Proposed RegQCNET

2.2.1. Implemented quantitative metric. In the scope of this study, we aim at quantifying the residual mis-alignment (noted T) between two given images via the Root Mean Square Error criterion (RMSE) computed as follows (Maurer et al. 1997):

$$\text{RMSE} = \frac{1}{\text{Card}(\Omega)} \sum_{\vec{r} \in \Omega} \sqrt{u(\vec{r})^2 + v(\vec{r})^2 + w(\vec{r})^2} \quad (1)$$

$\vec{r} = (x, y, z)$ being the voxel coordinates, Ω the image coordinates domain and $T = (u, v, w)$ the voxelwise 3D residual displacement vector field.

The proposed RegQCNET is thus designed to predict registration RMSE using two given images: a reference template and a registered one.

2.2.2. Implemented deep neural network. Figure 2 describes the architecture of the proposed quantitative CNN-based QC for image-to-template registration. Input images were first down-sampled by a factor 4 (note that a down-sampling factor 2 was also tested and discussed). We used a convolutional encoder followed by a 3 regression layers per resolution level using a basis of 24 filters of $3 \times 3 \times 3$ (*i.e.*, 24 filters for the first layer, 48 for the second and so on). Each block was composed of batch normalization, convolution and ReLU activation. We employed the following parameters: batch size = 1, optimizer = Adam with default parameters, epoch = 100, loss = Mean Square Error (MSE) and dropout = 0.5 after each block. We used 2 input channels (the down-sampled T1w and the template image).

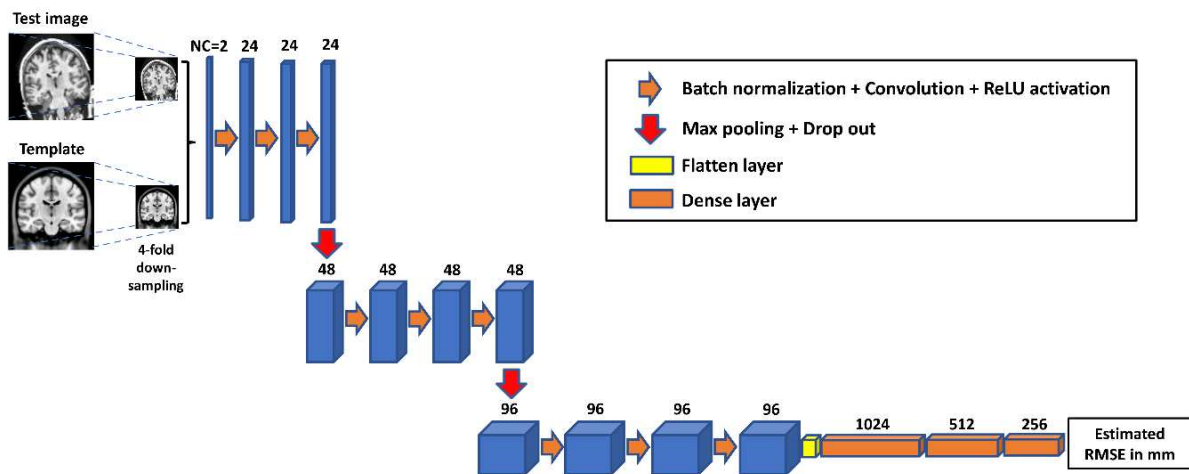


Figure 2: Architecture of the proposed RegQCNET for image-to-template registration. Each block is composed of batch normalization, convolution and ReLU activation. The number of input channels (NC) as well as the number of $3 \times 3 \times 3$ filters are indicated on the top of each block.

2.3. Experimental setup.

2.3.1. Assessment of RegQCNET on the “Simulated testing dataset”. For this dataset, we could benefit from the knowledge of real RMSEs. RegQCNET estimates were thus challenged against real RMSEs by evaluating R^2 , slope and Y-intercept of a linear regression: while the R^2 provides information about the precision of the proposed QC, the slope and Y-intercept allows quantifying its accuracy. We compared results obtained using three so-called “Simulated training datasets” (*i.e.*, with $N=100$, 1000 and 10000, respectively) for training. The robustness of RegQCNET were subsequently analyzed with spatially homogeneous and heterogeneous image intensity bias as follows:

Robustness against a spatially homogeneous intensity bias. RegQCNET was challenged against an homogeneous spatial intensity variation applied on all scans included in the testing dataset. For this purpose, the test scans were identically disturbed as follows: Let MAX_INTENSITY be the maximum intensity of an image I , and J be the image I after application of the spatially homogeneous intensity bias. For all voxel location \vec{r} , the intensity $I(\vec{r})$ was multiplied by a factor 2, while being restricted in the interval original intensity range $[0, \text{MAX_INTENSITY}]$:

$$J(\vec{r}) = \begin{cases} I(\vec{r}) \times 2 & \text{if } I(\vec{r}) \times 2 < \text{MAX_INTENSITY} \\ \text{MAX_INTENSITY} & \text{otherwise} \end{cases} \quad (2)$$

Robustness against a spatially heterogeneous intensity bias. RegQCNET was challenged against an heterogeneous spatial intensity variation applied on all scans included in the testing dataset. For this purpose, the test scans were identically disturbed as follows: Let $\vec{r}_0 = (x_0, y_0, z_0)$ be the voxel coordinates at the central position of an image I , and K be the image I after application of the spatially heterogeneous intensity bias. For all voxel location \vec{r} , the intensity $I(\vec{r})$ was weighted by a voxel-wise exponential decay as follow:

$$K(\vec{r}) = I(\vec{r}) \times \exp\left(-\frac{\|\vec{r} - \vec{r}_0\|_2^2}{2\sigma^2}\right) \quad (3)$$

Practically, intensities in voxels located close to the central position \vec{r}_0 were less disturbed than those located further. In the scope of this study, we took $\sigma = 60$.

2.3.2. Assessment of RegQCNET on the “Real testing dataset”. All 3953 brain images were visually inspected to build a gold standard QC. 13 mis-registered brain images were detected and considered as a “negative case” for the rest of the manuscript. The so-called “Simulated training dataset” with $N = 10000$ was here employed for training. The accuracies, area under the ROC curve (AUROC), sensitivity, specificity, positive predictive values (PPVs) and negative predictive values (NPVs) of the quantitative analysis were recorded for the following experiments:

Manually defined threshold. RegQCNET was used as an input feature to differentiate between scans with RMSE below and higher a user-defined classification threshold noted δ (δ was expressed in millimeters). We tested δ -values in the following set: $\{5, 10, 20, 50\}$ mm. The AUROC was here computed using the method detailed in (Cantor & Kattan 2000).

Automatically defined threshold. A 10-fold-stratified cross-validation was used to evaluate the performance of RegQCNET when using an threshold automatically tuned by machine learning algorithm. The dataset of 3953 brains was randomly partitioned into complementary 90%-training and 10%-test subsets (making sure that at least one positive and one negative case were included in each subset). For this purpose, the following classification algorithms were applied using the commercial software Matlab (©1994-2020 The MathWorks, Inc.)/"Statistics and Machine Learning" toolbox: logistic regression (LR), support vector machine (SVM), naïve bayes (NB) and random forest (RF). Default hyperparameters in Matlab implementations were employed for RF and SVM (RF: Classification method/100 bagged decision trees, SVM: supports sequential minimal optimization/box constraint/linear kernel) (Kohavi 1995). The cross-validation steps were repeated 1000 times with shuffling of the folds and test metric averages, standard deviations and confident intervals calculated.

Comparison with usual image features. The last above-mentioned study was also conducted using correlation coefficient (CC) and mutual information (MI) for comparison.

2.4. Hardware and implementation details.

We evaluated the computational burden of our proposed method using an Intel Xeon E5-2683 2.4 GHz (2 Hexadeca-core) with 256 GB of RAM equipped by a GPU Nvidia Tesla V100. The computation time during the testing session was evaluated without and with the use of the GPU. Our implementation was performed using Tensorflow 1.4 and keras 2.2.4.

3. Results

Fig. 3 shows typical images generated for the benchmark of the proposed CNN-based quantitative QC. Middle transversal, coronal and sagittal slices are reported for several 3D volumes. The template used as reference for affine image registration (see section 2.1.1) is displayed in the first row. The second (scan #1) row shows 3D brain images from the original lifespan dataset (RMSE considered equal to 0 mm). Lower rows (scan #[3 – 5]) show examples of 3D scans obtained after the application of simulated spatial transformations of various amplitudes, as described in section 2.1.2.

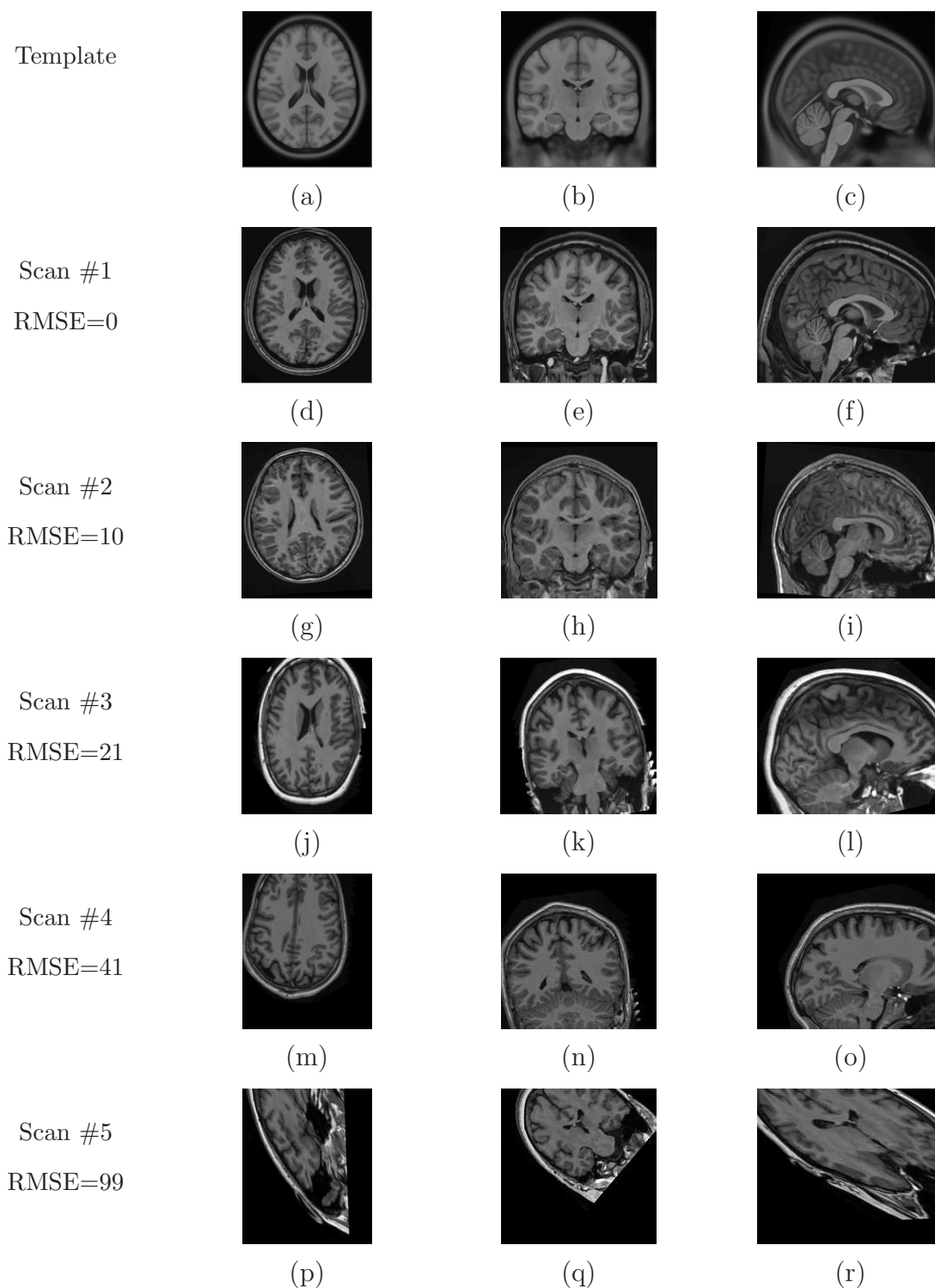


Figure 3: Typical images generated for the benchmark of the proposed CNN-based quantitative QC. Transversal (left column), coronal (middle column) and sagittal (right column) center cross-sections are reported for the template scan (a-c) and for different patients/various RMSE values. Each generated image is referred to as “Scan #[1 – 5]”.

3.1. Assessment of RegQCNET on the “Simulated testing dataset”.

Fig. 4 reports the precision and the accuracy of RegQCNET estimates obtained on the simulated test dataset (as described in section 2.1.2) using a simulated training dataset populated by 100 (4a), 1000 (4b) and 10000 (4c) scans. As one can expect, the precision (rated by the R^2 of the linear fit) improves when the size of the training dataset increased: the R^2 converged slowly toward 1 along with the size of the training dataset increased (R^2 equal to 0.84, 0.95 and 0.99 were obtained using 100, 1000 and 10000 images, respectively). The accuracy (rated by the slope and the Y-intercept of the linear regression) follows the same trend: RegQCNET under-estimated the RMSE (the slope of the linear regression was equal to 0.66) using a training dataset populated by $N = 100$ scans. However, as long as N increased, the slope and the Y-intercept converged toward optimal values (*i.e.*, 1 and 0, respectively).

Fig. 5 shows the impact of a spatial intensity bias (as described in section 2.1.2) on the performance of the proposed RegQCNET. While a spatially homogeneous intensity bias did not deteriorate the precision ($R^2=0.99$) and the accuracy (slope=0.98/Y-intercept=-1.08) (5c), this observation did not applied using a spatially heterogeneous bias (5e): in this last case, both precision ($R^2=0.98$) and accuracy (slope=0.89/Y-intercept=7.54) were slightly worse.

3.2. Assessment of RegQCNET on the “Real testing dataset”.

Fig. 6 shows a visualisation of RegQCNET-based RMSEs estimated for the 3953 tested brain MRIs. Transversal cross-section of mis-registered images, as detected by our visual inspection, are reported above and below the graph. These images can be visually compared to the corresponding template cross-section reported in Fig. 3a. In two images (referred to as case #9 and case #11 in Fig. 6) of patients with Alzheimer’s Disease, very large lateral ventricle slightly disturbed the registration, which had in turn a small impact on RegQCNET estimates (< 20 mm). In the 9 other images, huge mis-registrations are observable, which had in turn a high impact on RegQCNET estimates (> 50 mm).

3.2.1. Manually defined threshold. Table 1 reports classification scores of RegQCNET using all tested manually defined thresholds. A classification threshold $\delta = 10$ mm provided best scores: accuracy=99.6%, AUROC=1.0, sensitivity=99.6%, specificity=100.0%, PPV=100.0%, and NPV=44.8% (note that NPV=44.8% means here that 16 good-registered images were considered as mis-registered). Good- and mis-registered images were thus correctly identified in 3924/3940 and 13/13 brain images, respectively.

3.2.2. Automatically defined threshold. The RegQCNET output served as a metric in all tested machine learning classifiers (see Table 2). In particular, using the logistic regression classifier applied on the proposed RegQCNET, QC scores were:

accuracy=96.0%, AUROC=1.0, sensitivity=95.9%, specificity=100.0%, PPV=97.5%, and NPV=93.7%.

3.2.3. *Comparison with usual image features.* Very poor scores were obtained using CC (best classifier=naïve bayes) and MI (best classifier=logistic regression): a good detection of correctly registered images was achievable by accepting a large amount of false-negative cases, as shown in Fig. 7. Conversely, a perfect detection of mis-registered images was only achievable by accepting a dramatic impact on the sensitivity (*i.e.*, 1.7% and 30.9% for CC and MI, respectively, as shown in Table 2).

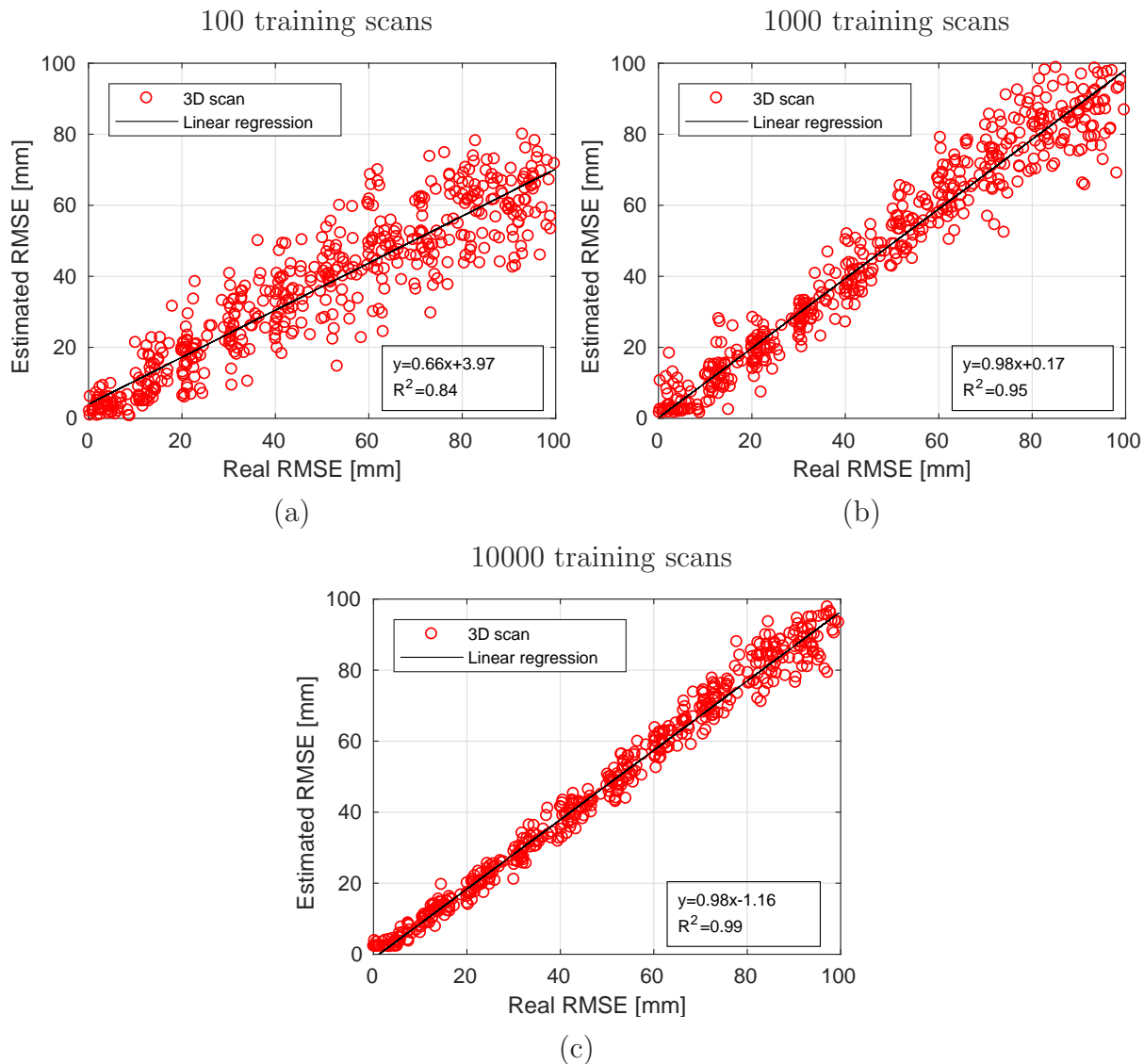


Figure 4: Typical CNN-based RMSE estimates obtained on the simulated dataset using training set composed by 100 (a), 1000 (b) and 10000 (c) scans. Estimated RMSEs are plotted against real RMSEs and the R^2 , slope and Y-intercept of a linear regression are reported in the insert of each graph.

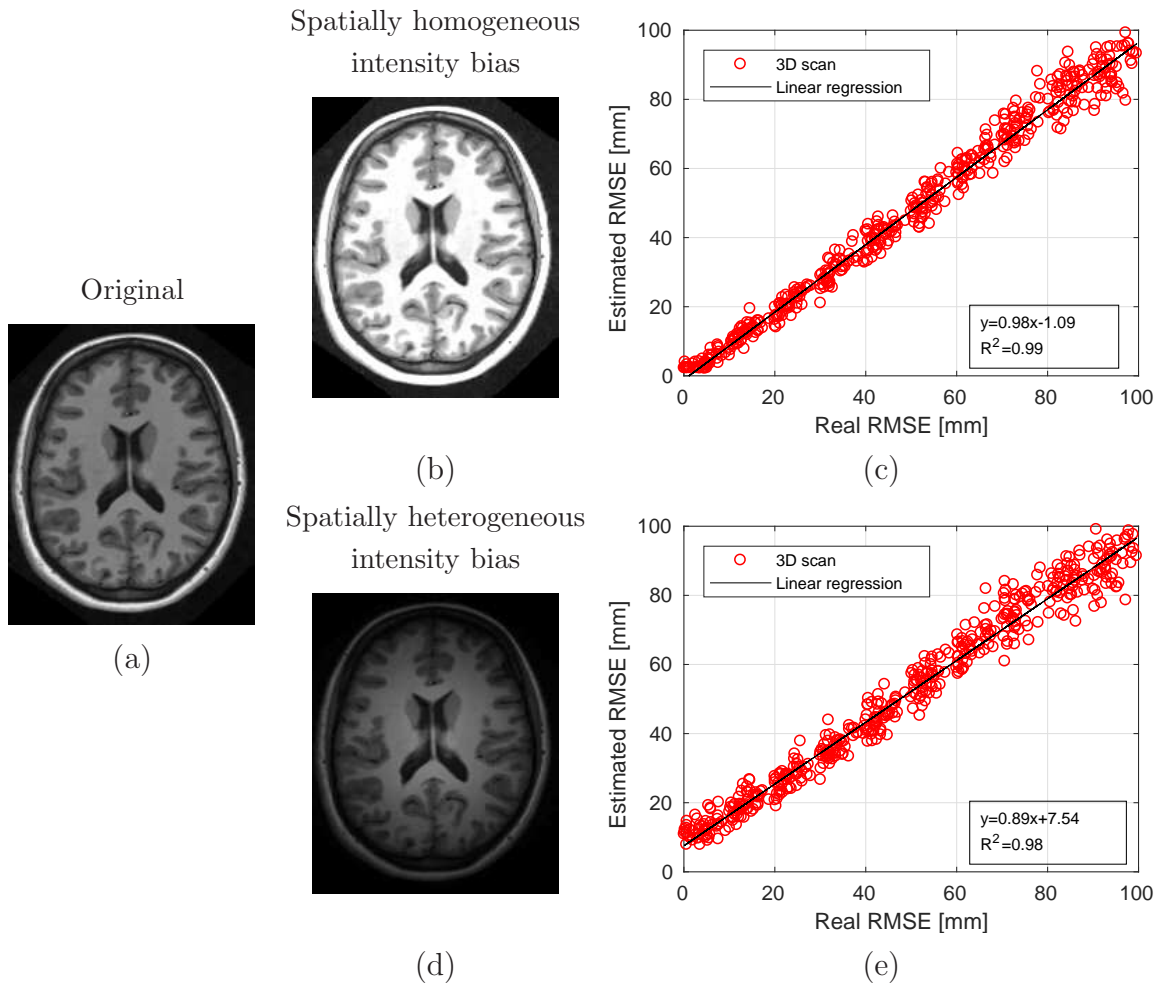


Figure 5: Typical CNN-based RMSE results obtained on the simulation experiment when a spatial intensity bias is applied on the testing dataset. A training dataset composed by 10000 scans (no spatial intensity bias) was used. The transversal center cross-section of a brain scan is reported before (a) and after application of an homogeneous (b) and an heterogeneous (d) intensity bias. Estimated RMSEs are plotted against real RMSEs for the homogeneous (c) and the heterogeneous (e) bias, and the R^2 , slope and Y-intercept of a linear regression is reported in the insert of each graph.

4. Discussion

The proposed method aims at quantifying the amplitude of the spatial affine mismatch between an image of the brain and a template. For this purpose, the RMSE criterion after registration was employed in the scope of this study. A quantitative (computer-assisted) approach delivers reproducible results and minimises operator dependency, as qualitative (visual) interpretation of mis-registered images lacks a learning curve when the process is automated.

It can be observed that good scores were obtained in both simulated and real datasets by well balanced training population covering the entire lifespan and uniformly

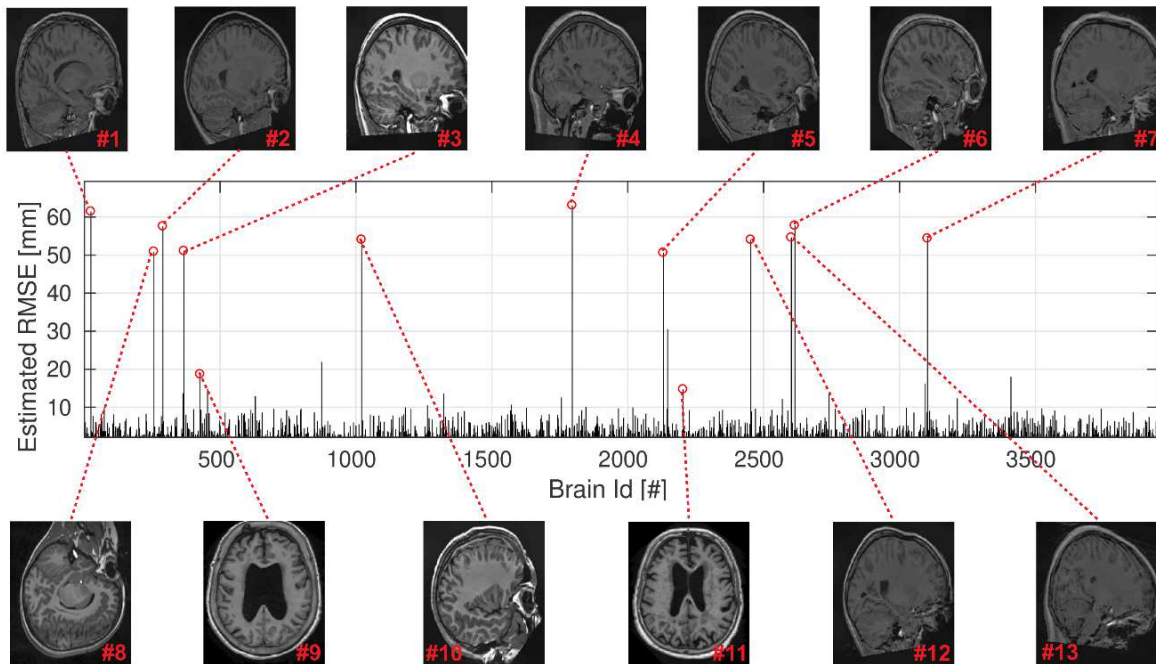


Figure 6: Visualisation of RegQCNET-based RMSEs estimated for the 3953 brains of the data base. Mis-registered images (transversal), as detected by our visual inspection, are reported above and below the graph. The corresponding template cross-section is shown in Fig. 3a.

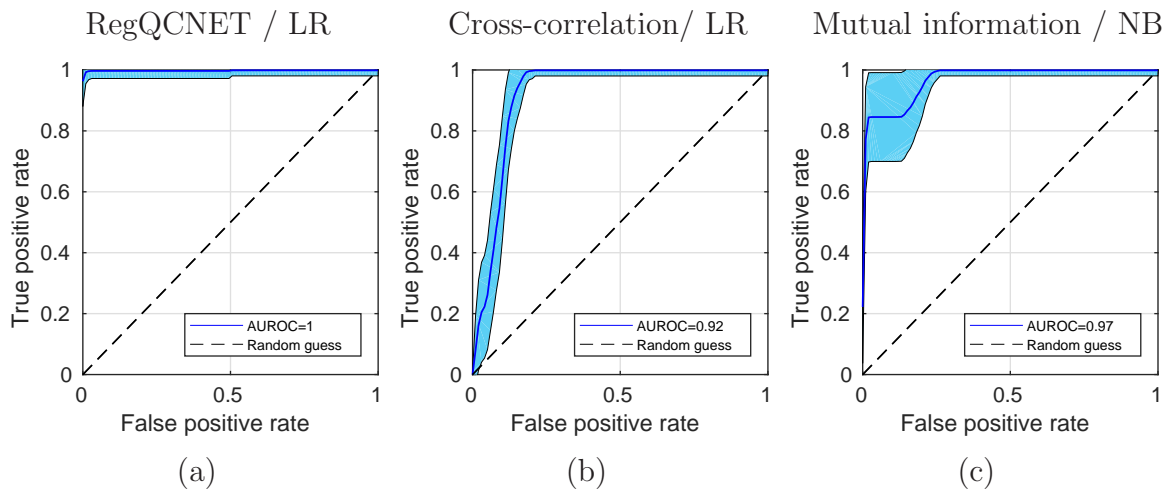


Figure 7: ROC curves obtained using the three tested indicators (RegQCNET (a), CC (b) and MI (c)) as binary classifiers (LR (a), LR (b) and NB (c)) for the two image populations (*i.e.*, correctly registered vs. mis-registered) after 10-fold cross-validation.

distributed amplitudes of random affine transformations. It is interesting to underline that comparable precision and accuracy were obtained on simulated data (as described in section 2.1.2) using a subsampling factor 2 on the images (instead of the subsampling factor 4 used in the shown results).

Classification scores: Manually defined threshold						
Classification threshold (δ) [mm]	Accuracy	AUROC	Sensitivity	Specificity	PPV	NPV
5	91.6	0.96	91.6	100.0	100.0	3.8
10	99.6	1.00	99.6	100.0	100.0	44.8
20	99.9	0.92	99.9	84.6	99.9	84.6
50	99.9	0.92	100.0	84.6	99.9	100.0

Table 1: Classification scores of the proposed RegQCNET on the “Real testing dataset”. Quantitative scores (*i.e.*, computer-assisted) are given, assuming the qualitative inspection (*i.e.*, visual) as a gold standard. AUROC: area under the ROC curve; PPV: positive predictive value; NPV: negative predictive value. Accuracies, sensitivities, specificities, PPVs, and NPVs are shown in percentages. Best performance are reported in bold font.

One can distinguish two potential contributions on the apparent image-to-template mismatch: (i) the effective registration error that we aim to quantify ; (ii) the anatomical variability between the actual image and the template (in particular, the size of the brain varies a lot along the lifespan). Any unobserved spatial transformation/brain shape during the training step may disturb in turn the proposed quantitative CNN-based QC. This phenomenon can be observed in Fig. 4a where an unsufficiently populated training dataset was employed (100 images), which increased the amount of unseen inter-subject variability of spatial transformation during the training session. In turn, a dramatic impact arise on both precision and accuracy.

Another limitation arise when a spatial intensity bias occurs between training and testing. While a spatially homogeneous didn’t hamper the performance (Fig. 5c), an accurate correction of spatially heterogeneous intensity bias is a necessary prerequisite for the successful achievement of RegQCNET (Fig. 5e) (Tustison et al. 2010) (Nyúl et al. 2000). It has to be noted that our framework was robust to defacing (*e.g.*, NDAR dataset) at testing time while trained without defacing.

As one can expect, the observation window for spatial transformations during training has to be carefully determined. That brings us to an inherent limit of the proposed technique: a RMSE extrapolation outside training limits is intrinsically not possible using our CNN-based approach and a large observation window is mandatory. This limitation could be limited by training RegQCNET on a larger range of RMSE.

Using the proposed CNN-based QC, a few tenth of a seconds (700 ms and 200 ms without and with the use of GPU acceleration, respectively) is needed to provide a quantitative prediction of the image-to-template alignment RMSE using our test platform. This perfectly meets our computational requirements related to the inclusion of this QC step in any analysis pipeline.

Classification scores: Automatically defined threshold						
Classifier	Accuracy	AUROC	Sensitivity	Specificity	PPV	NPV
RegQCNET						
LR	96.0±17.3 (94.7-97.2)	1.00±0.06 (0.99-1.00)	95.9±17.4 (94.7-97.2)	100.0±0.0 (100.0-100.0)	97.5±15.7 (96.4-98.6)	93.7±24.2 (92.0-95.4)
SVM	94.8±18.8 (93.4-96.1)	1.00±0.04 (1.00-1.00)	94.8±18.9 (93.4-96.1)	100.0±0.0 (100.0-100.0)	97.3±16.2 (96.1-98.5)	91.3±28.1 (89.3-93.3)
NB	85.7±34.1 (83.3-88.1)	1.00±0.04 (1.00-1.00)	85.6±34.2 (83.2-88.1)	100.0±0.0 (100.0-100.0)	86.8±33.9 (84.4-89.2)	84.0±36.6 (81.4-86.6)
RF	84.8±30.7 (75.7-93.9)	0.94±0.18 (0.89-1.00)	84.8±30.8 (75.6-93.9)	100.0±0.0 (100.0-100.0)	91.3±28.5 (82.8-99.8)	76.2±42.9 (63.5-89.0)
CC						
LR	0.8±6.0 (0.4-1.2)	0.92±0.05 (0.92-0.92)	1.7±12.4 (0.8-2.5)	100.0±0.0 (100.0-100.0)	0.7±8.4 (0.1-1.3)	0.6±5.2 (0.2-1.0)
SVM	0.6±3.9 (0.4-0.9)	0.76±0.32 (0.74-0.79)	0.7±7.4 (0.2-1.3)	100.0±0.0 (100.0-100.0)	0.9±9.3 (0.1-1.7)	0.3±0.0 (0.3-0.3)
NB	0.6±3.2 (0.4-0.9)	0.92±0.05 (0.91-0.92)	1.1±9.4 (0.4-1.8)	100.0±0.0 (100.0-100.0)	1.0±9.9 (0.3-1.7)	0.3±0.0 (0.3-0.3)
RF	0.3±0.0 (0.3-0.3)	0.48±0.06 (0.47-0.50)	0.0±0.0 (0.0-0.0)	100.0±0.0 (100.0-100.0)	0.0±0.0 (0.0-0.0)	0.3±0.0 (0.3-0.3)
MI						
LR	30.3±40.8 (27.4-33.2)	0.97±0.06 (0.96-0.97)	30.1±41.0 (27.2-33.0)	100.0±0.0 (100.0-100.0)	38.9±48.8 (35.4-42.4)	20.8±40.2 (18.0-23.7)
SVM	8.9±24.9 (7.2-10.7)	0.54±0.44 (0.50-0.57)	8.6±24.9 (6.9-10.4)	100.0±0.0 (100.0-100.0)	12.6±33.2 (10.2-15.0)	5.3±21.7 (3.8-6.9)
NB	30.9±41.0 (28.0-33.8)	0.97±0.07 (0.96-0.97)	30.9±41.3 (28.0-33.8)	100.0±0.0 (100.0-100.0)	39.8±49.0 (36.3-43.4)	21.0±40.4 (18.1-23.9)
RF	27.9±40.2 (18.9-36.9)	0.75±0.23 (0.70-0.80)	27.6±40.4 (18.6-36.7)	100.0±0.0 (100.0-100.0)	36.7±48.5 (25.8-47.6)	20.6±40.3 (11.5-29.6)

Table 2: Classification scores of the various classifiers on the “Real testing dataset”. Quantitative scores were derived via evaluation of RegQCNET, correlation coefficient (CC), and mutual information (MI) (after 10-fold cross-validation) by various machine-learning algorithms (LR: logistic regression, SVM: support machine vector, NB: naïve bayes, RF: random forest). Quantitative indicators are shown with standard deviations and 95% confidence intervals in parentheses. Best performance are reported in bold font for each indicator.

5. Conclusion

This study demonstrates that quantitative estimation of registration mismatch between a brain image and a template can be estimated using CNNs. However, to ensure the quality of the estimation, the training dataset have to be carefully designed. To this end, in this study we used: i) a gender and age well-balanced lifespan dataset covering the entire lifespan ; ii) uniformly distributed amplitudes of random spatial transformations to cover registration error from 0 to 100 millimeters ; iii) a sufficient range of amplitude for the simulated spatial transformations. The proposed tool can be used as quality control for automated image registration of patient T1-weighted brain scans onto a reference template.

Future studies will include the extension of the proposed RegQCNET for complex elastic (voxelwise) image deformations, the estimation of voxelwise RMSE maps, the impact of incomplete, noisy and corrupted brains, as well as the extension of the method to cross-contrast and multi-modal images.

Acknowledgment

Experiments presented in this paper were carried out using the PlaFRIM experimental testbed, supported by Inria, CNRS (LABRI and IMB), Université de Bordeaux, Bordeaux INP and Conseil Régional d’Aquitaine (see <https://www.plafrim.fr/>). This work benefited from the support of the project DeepvolBrain of the French National Research Agency (ANR-18-CE45-0013). This study was achieved within the context of the Laboratory of Excellence TRAIL ANR-10-LABX-57 for the BigDataBrain project. Moreover, we thank the Investments for the future Program IdEx Bordeaux (ANR-10-IDEX-03-02, HL-MRI Project), Cluster of excellence CPU and the CNRS/INSERM for the DeepMultiBrain project. This study has been also supported by the DPI2017-87743-R grant from the Spanish Ministerio de Economía, Industria Competitividad. The authors gratefully acknowledge the support of NVIDIA Corporation with their donation of a TITAN X GPU used in this research.

References

- Alfaro-Almagro, F., Jenkinson, M., Bangerter, N. K., Andersson, J. L. R., Griffanti, L., G., D., Sotiropoulos, S. N., Jbabdi, S., Hernandez-Fernandez, M., Vallee, E., Vidaurre, D., Webster, M., McCarthy, P., Rorden, C., Daducci, A., Alexander, D. C., H., Z., Dragonu, I., Matthews, P. M., Miller, K. L. & Smith, S. M. (2018). Image processing and quality control for the first 10,000 brain imaging datasets from uk biobank, *NeuroImage* **166**: 400–424.
- Avants, B. B., Tustison, N. J., Song, G., Cook, P. A., A., K. & Gee, J. C. (2011). A reproducible evaluation of ants similarity metric performance in brain image registration, *NeuroImage* **54**(3): 2033–2044.
- Bannister, S. E., Page, D., Standen, T., Dunne, A., Rawling, J. P., Birch-Sykes, C. J., Wilson, M. Z., Holloway, S., McClelland, J. & Peters, Y. (2019). Deep neural networks for quality assurance of image registration.

- Cantor, S. B. & Kattan, M. W. (2000). Determining the area under the ROC curve for a binary diagnostic test, *Medical Decision Making* **20**(4): 468–470.
- Chaogan, Y. & Yufeng, Z. (2010). DPARSF: a MATLAB toolbox for "pipeline" data analysis of resting-state fMRI, *Frontiers in Systems Neuroscience* **4**: 13.
- Collins, D. L., Neelin, P., Peters, T. M. & Evans, A. C. (1994). Automatic 3d intersubject registration of MR volumetric data in standardized talairach space, *Journal of computer assisted tomography* **18**(2): 192–205.
- Cook, P., Bai, Y., Nedjati-Gilani, S., Seunarine, K., Hall, M., Parker, G. & Alexander, D. (2006). Camino: open-source diffusion-MRI reconstruction and processing, Vol. 2759, p. 2759.
- Coupé, P., Catheline, G., Lanuza, E. & Manjón, J. V. (2017). Towards a unified analysis of brain maturation and aging across the entire lifespan: A MRI analysis, *Human Brain Mapping* **38**(11): 5501–5518.
- Coupé, P., Manjón, J. V., Lanuza, E. & Catheline, G. (2019). Lifespan changes of the human brain in alzheimer's disease, *Scientific Reports* **9**(1): 3998.
- Dubost, F., de Bruijne, M., Nardin, M., Dalca, A., Donahue, K., Giese, A.K. aband Etherton, M., Wu, O., de Groot, M., Niessen, W. & Vernooij, M. (2019). Automated image registration quality assessment utilizing deep-learning based ventricle extraction in clinical data, **arXiv preprint arXiv:1907.00695**.
- Eppenhof, K. A. J. & Pluim, J. P. W. (2018). Error estimation of deformable image registration of pulmonary ct scans using convolutional neural networks, *Journal of Medical Imaging* **5**(2).
- Fonov, V., Evans, A. C., Botteron, K., Almli, C. R., McKinstry, R. C. & Collins, D. L. (2011). Unbiased average age-appropriate atlases for pediatric studies, *NeuroImage* **54**(1): 313–327.
- Fonov, V. S., Dadar, M. & Collins, D. L. (2018). Deep learning of quality control for stereotaxic registration of human brain MRI, *bioRxiv*.
- Friston, K. J., Ashburner, J., Frith, C. D., Poline, J. B., Heather, J. D. & Frackowiak, R. S. J. (1995). Spatial registration and normalization of images, *Human Brain Mapping* **3**(3): 165–189.
- Hessam, S., Saygili, G., Glocker, B., Lelieveldt, B. P. F. & Staring, M. (2019). Quantitative error prediction of medical image registration using regression forests, **abs/1905.07624**.
- Jenkinson, M., Beckmann, C. F., Behrens, T. E., Woolrich, M. W. & Smith, S. M. (2012). FSL, *NeuroImage* **62**(2): 782–790.
- Kim, H., Irimia, A., Hobel, S. M., Pogosyan, M., Tang, H., Petrosyan, P., Blanco, R. E. C., Duffy, B. A., Zhao, L., Crawford, K. L., Liew, S. L., Clark, K., Law, M., Mukherjee, P., Manley, G. T., Van Horn, J. D. & Toga, A. W. (2019). The LONI QC system: A semi-automated, web-based and freely-available environment for the comprehensive quality control of neuroimaging data, *Frontiers in Neuroinformatics* **13**: 60.
- Kohavi, R. (1995). A study of cross-validation and bootstrap for accuracy estimation and model selection, pp. 1137–1143.
- Manjón et al., J. V. (2008). Robust MRI brain tissue parameter estimation by multistage outlier rejection, *Magnetic Resonance in Medicine: An Official Journal of the International Society for Magnetic Resonance in Medicine* **59**(4): 866–873.
- Manjón, J. V. & Coupé, P. (2016). volbrain: An online MRI brain volumetry system, *Frontiers in neuroinformatics* **10**: 30.
- Manjón, J. V., Coupé, P., L. M.-B. D. L. C. & Robles, M. (2010). Adaptive non-local means denoising of MR images with spatially varying noise levels, *Journal of Magnetic Resonance Imaging* **31**(1): 192–203.
- Maurer, C. R. J., Fitzpatrick, J., Wang, M., Galloway, R. L. J., Maciunas, R. & Allen, G. (1997). Registration of head volume images using implantable fiducial markers, *IEEE Transactions on Medical Imaging* **16**: 447–462.
- Nyúl, L. G., Udupa, J. K. & Zhang, X. (2000). New variants of a method of MRI scale standardization, *IEEE Transactions on Medical Imaging* **19**: 143–150.
- Sled, J. G., Zijdenbos, A. P. & Evans, A. C. (1998). A nonparametric method for automatic correction

- of intensity nonuniformity in MRI data, *IEEE Transactions on Medical Imaging* **17**(1): 87–97.
- Song, X. W., Dong, Z. Y., Long, X. Y., Li, S. F., Zuo, X. N., Zhu, C. Z., He, Y., Yan, C. G. & Zang, Y. F. (2011). REST: a toolkit for resting-state functional magnetic resonance imaging data processing, *PLoS One* **6**(9): e25031.
- Tustison, N., Avants, B. B., Cook, P. A., Zheng, Y., Egan, A., Yushkevich, P. A. & Gee, J. C. (2010). N4itk: Improved n3 bias correction, *IEEE Transactions on Medical Imaging* **29**(6): 1310–1320.
- Tustison, N. J., Cook, P. A., Klein, A., Song, G., Das, S. R., Duda, J. T., Kandel, B. M., van Strien, N., Stone, J. R., Gee, J. C. & Avants, B. B. (2014). Large-scale evaluation of ants and freesurfer cortical thickness measurements, *NeuroImage* **99**: 166–179.
- Wei, X., Warfield, S. K., Zou, K. H., Wu, Y., Li, X., Guimond, A., Mugler, J. P., Benson, R. R., Wolfson, L., Weiner, H. L. & R., G. C. (2002). Quantitative analysis of MRI signal abnormalities of brain white matter with high reproducibility and accuracy, *Journal of Magnetic Resonance Imaging* **15**(2): 203–209.